

Received June 30, 2020, accepted July 10, 2020, date of publication July 14, 2020, date of current version July 24, 2020.

Digital Object Identifier 10.1109/ACCESS.2020.3009161

Underwater Image Enhancement Based on Global and Local Equalization of Histogram and Dual-Image Multi-Scale Fusion

LINFENG BAI^{ID}¹, WEIDONG ZHANG^{ID}^{1,2}, (Student Member, IEEE),

XIPENG PAN^{ID}³, AND CHENPING ZHAO^{ID}¹

¹School of Information Engineering, Henan Institute of Science and Technology, Xinxiang 453003, China

²School of Information Science and Technology, Dalian Maritime University, Dalian 116026, China

³School of Computer Science and Information Security, Guilin University of Electronic Technology, Guilin 541004, China

Corresponding author: Weidong Zhang (zwd_wd@163.com)

This work was supported in part by the National Natural Science Foundation of China under Grant 61906050, in part by the Guangxi University Young and Middle-Aged Teachers' Research Ability Improvement Project under Grant 2020KY05034, and in part by the Science Research Foundation of the Guilin University of Electronic Science and Technology under Grant UF20001Y.

ABSTRACT Underwater images suffer from color cast and low visibility caused by the medium scattering and absorption, which will reduce the use of valuable information from the image. In this paper, we propose a novel method which includes four stages of pixel intensity center regionalization, global equalization of histogram, local equalization of histogram and multi-scale fusion. Additionally, this method uses a pixel intensity center regionalization strategy to perform centralization of the image histogram on the overall image. Global equalization of histogram is employed to correct color of the image according to the characteristics of each channel. Local equalization of dual-interval histogram based on average of peak and mean values is used to improve contrast of the image according to the characteristics of each channel. Dual-image multi-scale fusion to integrate the contrast, saliency and exposure weight maps of the color corrected and contrast enhanced images. Experiments on variety types of degraded underwater images show that the proposed method produces better output results in both qualitative and quantitative analysis, thus, the proposed method outperforms other state-of-the-art methods.

INDEX TERMS Underwater image enhancement, pixel intensity center regionalization, histogram equalization, multi-scale fusion.

I. INTRODUCTION

In recent years, with the continuous growth of population and the shortage of resources, people have turned their attention to the development and utilization of the ocean world with rich mineral resources. However, the water medium and the suspended particles have absorption and scattering effect on light when traveling in water [1]–[3]. Absorption causes color distortion of underwater images, while scattering results in low visibility of underwater images. In brief, the visual degeneration of underwater images is multifarious in Figure 1. Therefore, the study of underwater sharpening technology is of great significance for the exploration and utilization of underwater resources [4]–[6].

To improve the quality of underwater degraded images, underwater sharpening methods include underwater image

The associate editor coordinating the review of this manuscript and approving it for publication was Andrea F. Abate ^{ID}.

restoration methods, underwater image enhancement methods and data-driven methods that are put forward successively. Restoration methods [13]–[24] consider the degraded physical model to restore underwater images. However, the restoration methods are inflexible to be implemented due to various complicated underwater physical and optical factors. Enhancement methods [25]–[45] focus on modifying pixel values to enhance underwater images without considering underwater imaging parameters. Although the enhancement methods are simple and fast, it tends to over-enhanced or under-enhanced due to failure to consider underwater optical imaging parameters. Data-driven methods [51]–[58] are trained to rely on synthetic pairs of degraded images and high-quality counterparts. However, the data-driven methods heavily depend on a lot of training data and complex network structures.

In this paper, a method based on global and local equalization of histogram and dual-image multi-scale fusion

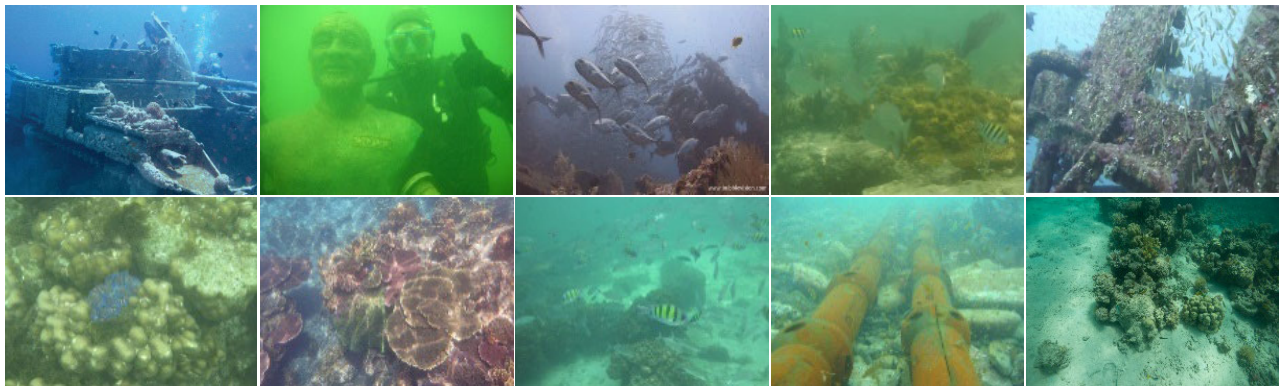


FIGURE 1. Examples of different underwater degraded images; these degraded underwater images are from [57].

(GLHDF) is proposed to enhance underwater images. First, a pixel intensity centered image is obtained from the input image via a Retinex-based inspired method. Then, a color-corrected is obtained from the centered image by a global equalization of histogram strategy and a contrast-enhanced image is obtained from the color-corrected image by a local equalization of dual-interval histogram based on average of peak and mean values strategy. Finally, a dual-image multi-scale fusion strategy is used to fuse the color-corrected and contrast-enhanced images. Quantitative and qualitative results demonstrate that the enhanced image achieves significant and sufficient improvements in color and contrast. The main contributions of this paper are summarized as:

1) A novel underwater image enhancement method based on global and local equalization of histogram and dual-image multi-scale fusion is proposed. It is suitable not only for variety types of degraded underwater images, but also for low-light, natural, foggy, and sandy images.

2) A pixel intensity center regionalization strategy is employed to perform centralization of the image histogram for each color channel. It not only smoothes the image, but also increases the similarity of the tricolor histogram.

3) A dual-interval histogram based on average of peak and mean values is applied to enhance the foreground sub-image and background sub-image, and then the contrast-enhanced image is integrated based on the average point.

4) A dual-image multi-scale fusion is used to fuse the color corrected image and contrast enhanced image to obtain a high-quality output image.

The rest of the paper is organized as follows. In section II, we review the progress of underwater image sharpening methods. Section III details the motivation of the proposed method. Section IV details the proposed method from pixel centralization, color correction, enhancement contrast and fusion. Section V shows the results of qualitative and quantitative comparison of the proposed and state-of-the-art methods. The last section summarizes the conclusions and future work of the study.

II. RELATED WORK

From different views, this paper summarizes the underwater image sharpening technology into three categories: underwater image restoration method, underwater image enhancement method and data-driven method.

A. UNDERWATER IMAGE RESTORATION METHOD

Underwater image restoration method restores underwater images by inverting the degraded process and estimating the parameters of the degraded model. Polarization-based methods [7]–[9] were applied to recover underwater images, which could improve the visibility and contrast of underwater images. However, it required hardware devices to obtain deep scene information of different degrees of polarization.

In recently, the dark channel prior (DCP) [10] had shown superiority in the field of image defogging [11], [12] and had been gradually applied to underwater image restoration [13]–[24]. Chiang and Chen [13] restored underwater images by a defogging method and a wavelength compensation method, it could handle light scattering and color distortions simultaneously. Galdran *et al.* [14] proposed an automatic red-channel method to restore color and improve contrast of the image. Drews *et al.* [15] presented an underwater dark channel prior (UDCP) restoration method by modifying the original DCP [10]. Li *et al.* [16] proposed an effective enhancement method based on histogram distribution prior and minimum information loss, which could improve the contrast and brightness of underwater images. In [17], a random forest regression model to estimate the transmission of underwater scenes was proposed. Peng and Cosman [18] proposed an underwater image restoration method based on image blurriness and light absorption. Peng *et al.* [19] proposed a generalized dark channel prior (GDCP) for underwater image restoration, which could be applied to foggy, hazy, sandstorm, and underwater images. Wang *et al.* [20] presented an underwater image restoration method based on adaptive attenuation-curve prior. Yang *et al.* [21] proposed a reflection-decomposition-based transmission map estimation underwater image restoration method.

In addition, haze-line-based [22] and color-line-based [23] methods were gradually applied to underwater restoration. Moreover, Berman *et al.* [22] constructed a distance maps dataset. Akkaynak and Treibitz [24] proposed a physically accurate model based on an atmospheric image formation model to enhance underwater image.

B. UNDERWATER IMAGE ENHANCEMENT METHOD

Underwater image enhancement method improves the contrast and brightness of underwater images by modifying pixel values of images. It mainly includes histogram-based [25]–[30], Retinex-based [31]–[34], fusion-based [35]–[39] and other methods [40]–[45]. Iqbal *et al.* [25] stretched the dynamic grey range in RGB color model and HSI color model to improve the contrast and color of underwater images. Ghani *et al.* [26] stretched the dynamic grey level in RGB color model and HSV color model to enhance the contrast and color of underwater images. Ghani and Isa [27] enhanced the low-quality underwater images by dual-image Rayleigh-stretched contrast-limited adaptive histogram. Ghani and Isa [28] modified the work of [26], [27] to improve underwater image contrast and color by recursive adaptive histogram modification. Shahrizan and Ghani [29] improved the visibility of underwater image by recursive-overlapped contrast limited adaptive histogram and dual-image wavelet fusion. Azmi *et al.* [30] proposed a color enhancement method based on natural underwater image, which mainly included underwater color cast neutralization, dual-intensity images fusion, swarm-intelligence based mean equalization and unsharp masking.

Underwater image enhancement based on the Retinex method. Fu *et al.* [31] proposed an underwater image enhancement method based on Retinex, it included color correction, layer decomposition, and enhancement. Zhang *et al.* [32] employed an extended multi-scale Retinex to enhance underwater images. Chong *et al.* [33] proposed an underwater image and video enhancement method based on Retinex. In [34], a multi-channel convolutional MSRCR method for enhancement of fog images and underwater images was proposed.

Underwater image enhancement based on the fusion method. Ancuti *et al.* [35] proposed a fusion-based strategy to enhance the visibility of underwater images, the weight maps consisted of luminance, contrast, chromatic, and saliency weight maps. Treibitz and Schechner [36] employed a multi-directional illumination fusion method for turbid scene enhancement. In [37], an underwater images and videos enhancement method based on fusion was proposed, which consisted of white balance and multi-scale fusion. Lu *et al.* [38] proposed an underwater image super resolution method based on descattering and fusion. Ancuti *et al.* [39] proposed a color balance and fusion method to underwater image enhancement.

Another line of research tries to enhance underwater images. Lu *et al.* [40] employed a weighted guided trigonometric filtering and artificial light correction for underwa-

ter image enhancement. Fu *et al.* [41] proposed a two-step method for single underwater image enhancement, which consisted of color correction and optimal contrast. In [42], an underwater image color correction method using exposure-bracketing imaging was proposed. In [43], an underwater image enhancement method based on adaptive retinal mechanisms was proposed. Ancuti *et al.* [44], [45] proposed a color channel transfer for image dehazing [44] and a color channel compensation for image enhancement [45], respectively.

C. DATA-DRIVEN METHOD

The superior performance of deep learning in image segmentation [46], image defogging [47], super resolution [48], and salient objection detection [49] had demonstrated in recent years. Moreover, deep learning-based methods were gradually applied to low-level vision problems [50], [51]. However, underwater imaging models were depended on specific scenes and lighting conditions. Therefore, it is difficult to generate a real-world underwater image by deep learning. In [51], the survey had concluded that the performance and the number of underwater image enhancement methods based on deep learning did not match the success of recent low-level vision problems based on deep learning.

Recently, Li *et al.* [52] proposed a real-time color correction method based on unsupervised generative network for monocular underwater images. Li *et al.* [53] proposed a weakly supervised underwater image color correction method based on cycle-consistent adversarial networks. Upalavikar *et al.* [54] presented a domain-adversarial learning for underwater image enhancement, which nicely handled the diversity of water. Chen *et al.* [55] proposed a GAN-based restoration scheme to improve the low contrast of underwater images, which developed a multibranch discriminator for the purpose of simultaneously preserving image content and removing underwater noise. Guo *et al.* [56] designed a new underwater image restoration model based on parallel convolutional neural network. Li *et al.* [57] constructed an underwater image enhancement benchmark (UIEB) and proposed an underwater image enhancement network trained on this benchmark, which including 950 read-world images, 890 of which had the corresponding reference images. An underwater scene prior method was proposed in [58], the UWCNN model generalized well to different underwater scenes as real-world and synthetic underwater images and videos. In additional, Liu *et al.* [59] designed an undersea image capturing system and constructed a large-scale real-world underwater image enhancement dataset divided into three subsets, and the three subsets target at three challenging aspects for enhancement, image visibility quality, color casts and higher-level detection/classification, respectively.

Although data-driven-based underwater image enhancement methods have achieved some achievements, these methods have complex network structures with long training times, and rely on large amounts of training data.

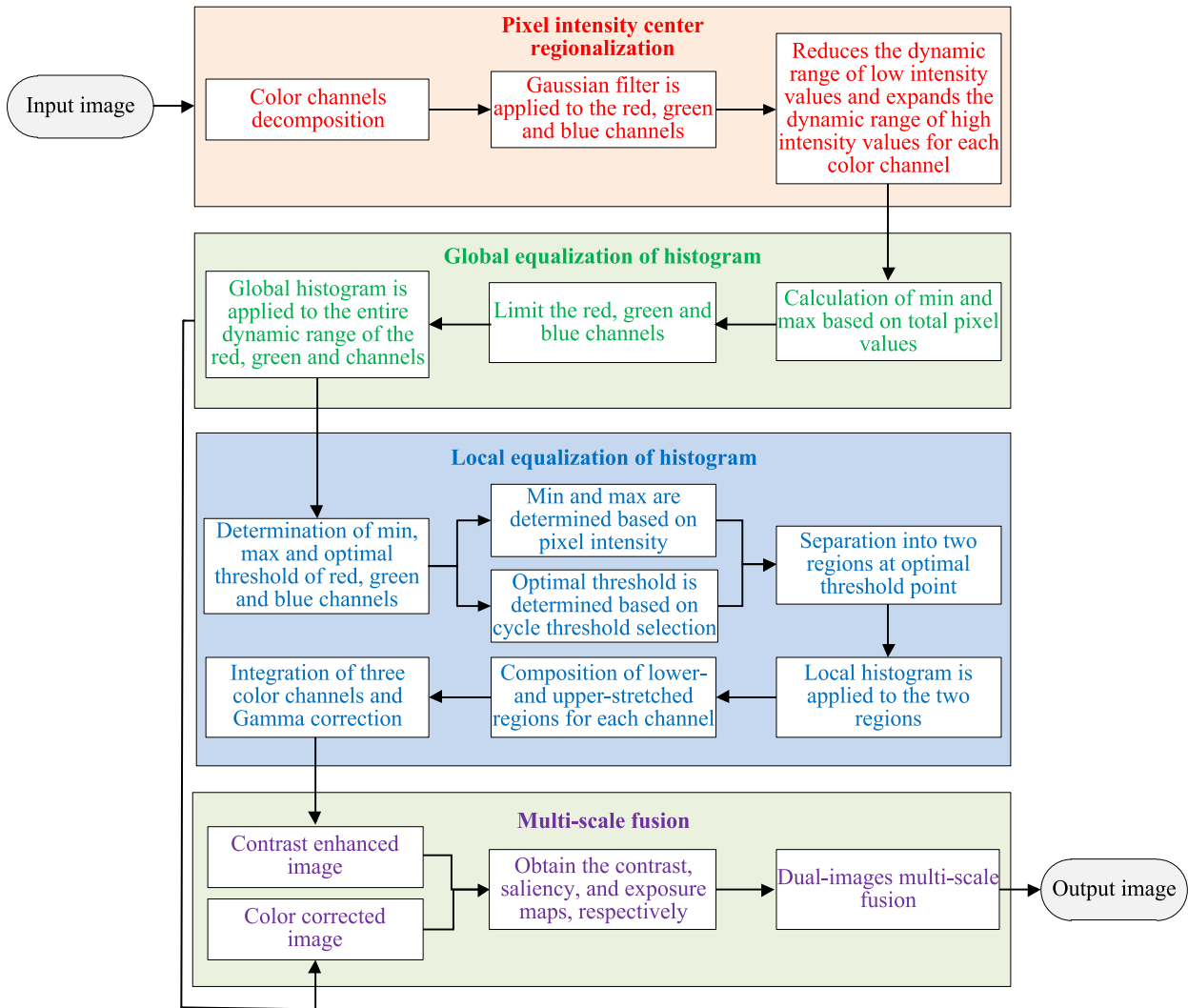


FIGURE 2. Flowchart of the proposed GLHDF method.

III. MOTIVATION

Underwater captured images suffer from random noise caused by the irregular movement of electronic components and photons during the imaging process. However, the noise interference affects the subsequent processing of underwater images. In addition, it also suffers from color cast and low visibility caused by the scattering and absorption. More seriously, the color cast and low visibility will reduce the use of valuable information from the image. Therefore, the noise, color cast, and low visibility are three issues that need to be addressed urgently for underwater degraded images.

In the noise study, such as guide filter [11], Gaussian filter [32], and trigonometric filter [40] all show the effectiveness of smoothing and denoising, but the complexity of the guide filter and trigonometric filter is higher than the Gaussian filter. Therefore, a Gaussian smoothed image is obtained from the input image using a Retinex-based inspired method, that is, a pixel intensity centered image is obtained. And then, we focus on color correction and contrast enhancement of the smoothed image in subsequent work.

In the color correction and contrast enhancement study, such as UCM [25] and ICM-RD [26] implement global enhancement in the process of considered the histogram modification of the overall image. Meanwhile, DIRS-CLAHS [27], RAHIM [28] and RO-CLAHS [29] consider the enhancement process by dividing the image into windows of the identical size. However, as the number of windows increases, the processing time also increases. NUCE [30] used dual-intensity images fusion method based on average of mean and median values without considering the processing of windows. Therefore, we consider not only global color correction based on UCM [25] and ICM-RD [26], but also local contrast enhancement based on NUCE.

On the one hand, the GLHDF method conducts global color correction by a global equalization of histogram strategy. The global equalization of histogram is different from the UCM [25] and ICM-RD [26], it performs linear transformation according to the characteristics of each color channel. On the other hand, the GLHDF method implements local contrast enhancement by dual-interval histogram based on

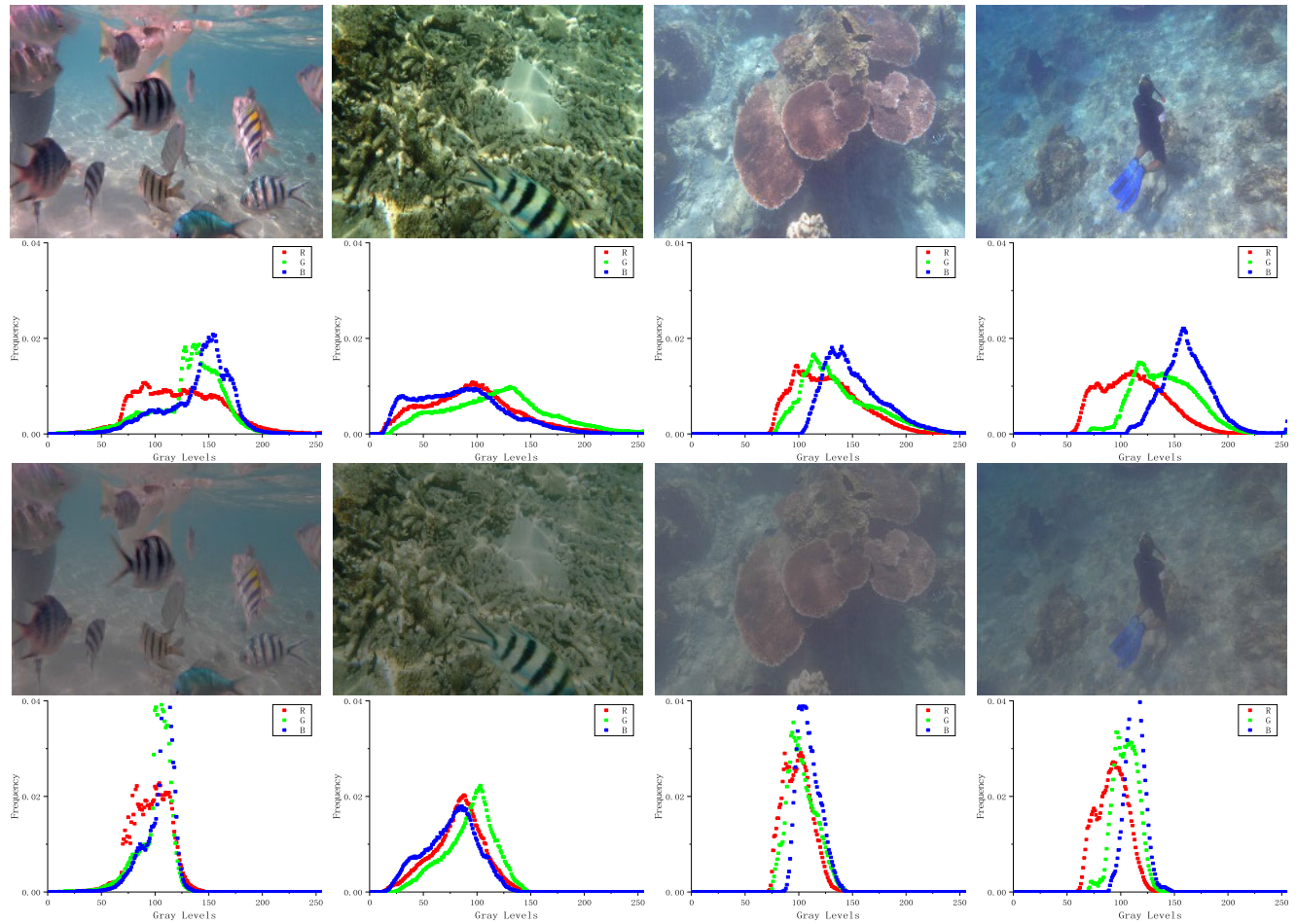


FIGURE 3. Pixel intensity centered underwater images. From top to bottom: 1. Raw underwater images; 2. Tricolor histogram corresponding to the first row; 3. Pixel intensity centered underwater images; 4. Tricolor histogram corresponding to the third row.

average of peak and mean values strategy. The dual-interval histogram is different from the dual-interval of the NUCE, which uses the average value equality strategy of foreground and background sub-images to obtain the dual-interval separation threshold. Finally, a dual-image multi-scale fusion strategy is used to fuse the color-corrected and contrast-enhanced images. The details of the proposed method are explained in the subsequent sections.

IV. METHODOLOGY

As illustrated in Figure 2, the proposed GLHDF method consists of four stages, namely, (1) Pixel intensity center regionalization (PICR), (ii) Global Equalization of Histogram (GEH), (iii) Local Equalization of Histogram (LEH), and (iv) Dual-image multi-scale fusion (DIMCF). The first step is to remove noise and smooth image by the multi-scale Gaussian filter. Meanwhile, the second step intends to correction color by global equalization of histogram strategy according to the characteristics of each color channel. The third step is implemented to improve the contrast of the color corrected image by the dual-interval histogram based on average of

peak and mean values. Finally, the enhanced underwater image is obtained by a dual-image multi-scale fusion strategy to integrate the color corrected and contrast enhanced images.

A. PIXEL INTENSITY CENTER REGIONALIZATION

Underwater captured images suffer from random noise caused by the irregular movement of electronic components and photons during the imaging process, it affects the color correction and contrast enhancement of underwater images seriously. Therefore, the noise removal from underwater images is of great application value. First, an underwater image in RGB color model are decomposed into its respective color channels. For each color channel, the image needs to be performed with Gaussian smoothing. In Retinex [32], a real-world image can be defined as

$$S(x, y) = L(x, y)^* R(x, y) \quad (1)$$

where $S(x, y)$ is the observed image, $L(x, y)$ and $R(x, y)$ are luminance and reflectance components, respectively. To separate the luminance $L(x, y)$ and reflectance $R(x, y)$, the

equation (1) needs to be converted to the log domain.

$$\log(S(x, y)) = \log(L(x, y)) + \log(R(x, y)) \quad (2)$$

In [32], it is required to reduce the effect of the luminance component $L(x, y)$ for further preserve the reflectance component $R(x, y)$ of the object. Gaussian low-pass filter, which allows low-frequency signals to pass while cutting off or attenuating high-frequency signals. In underwater image, the noise is regarded as high-frequency signal which is not required for further analysis. Therefore, Gaussian kernel functions with different scales are used to convolve the original image $S(x, y)$ to estimate the luminance component $L(x, y)$. Eq. (2) can be redefined as

$$R(x, y) = \sum_{n=1}^N w_n \{ \log(S(x, y)) - \log(G_n(x, y)^* S(x, y)) \} \quad (3)$$

where N is the number of scales, and $G_n(x, y) = \frac{1}{2\pi\sigma_n^2} \exp \frac{-(x^2+y^2)}{2\sigma_n^2}$. Typically, $0 \leq \sigma < 50$ is small scale, $50 \leq \sigma < 100$ is medium scale, and $100 \leq \sigma$ is large scale. The determination of N and σ_n refers to our previous defogging work [34]. Since the underwater scene is different from the foggy scene, we finally determined $\sigma_1 = 10$, $\sigma_2 = 30$, $\sigma_3 = 60$, $\sigma_4 = 80$, $\sigma_5 = 120$, $\sigma_6 = 160$, and $n = 6$ based on extensive experiments and experimental design references [34]. Then, Eq. (3) is implemented to each color channel.

The transformation operation of the Log domain improves the contrast of the image while smoothing the image (see the third row in Figure 3). In addition, it introduces a problem of color distortion. Therefore, a Gamma correction is introduced into Eq. (3) as follows

$$P_{out}(x, y) = 255^* \left(\frac{P_{in}(x, y)}{255} \right)^\gamma \quad (4)$$

where P_{in} and P_{out} are the input and output of pixel values, respectively. γ is constant, the Gamma correction has two main effects when $\gamma > 1$. On the one hand, it reduces the dynamic range of low grayscale areas to reduce the contrast of images in low grayscale areas. On the other hand, it expands the dynamic range of high grayscale areas to improve the contrast of images in high grayscale areas. Meanwhile, the overall contrast of the image is also reduced as shown in the third row of Figure 3. Finally, the Eq. (3) is redefined as

$$P_{out}(x, y) = 255^* \left(\frac{\sum_{n=1}^N w_n \{ \log(S(x, y)) - \log(G_n(x, y)^* S(x, y)) \}}{255} \right)^\gamma \quad (5)$$

where $\gamma = 3$ is determined based on a large number of statistical analyses. Figure 3 illustrates several examples of PICR. For pixel intensity centered underwater images, the tricolor histogram distribution is more concentrated and similar than the tricolor histogram distribution of raw underwater images. Despite the pixel intensity centered image

with low visibility and color distortion, the distribution of the tricolor histogram is more similar and the images are smoother from subjective visual perspective, which is desired in our framework. Therefore, the color and contrast of images need to be further improved. In sections B and C, we focused on the color correction and the contrast enhancement, respectively.

B. GLOBAL EQUALIZATION OF HISTOGRAM

In Figure 3, underwater image processed by PICR still with serious problems of color distortion and low visibility. The intensity distribution of the tricolor histogram is generally concentrated within a certain range of intensity level, that is, the tricolor histogram cannot be sufficiently distributed in the entire range of the intensity level. However, the PICR operation makes the pixel intensities of red, green, and blue channels more similar. Therefore, the color of image is corrected by applying a global equalization strategy of histogram correction to each color channel. The pixels of the image are distributed widely within the entire range of the intensity level. However, the intensity level of the output is limited to per^c of the minimum and maximum limits in the global equilibrium strategy. The limit strategy is used to reduce the effects of under- and over-corrected areas in the image.

1) Calculation the minimum and maximum values of histograms of red, green, and blue channels.

First, the histogram of red, green, and blue channels is calculated. Then, the limited ratio per^c corresponding to the minimum and maximum intensity is defined as Eq. (8), that is, the limit ratio per^c is determined based on the relationship between the total pixel intensity of each channel. Unlike the limit ration of [26] and [27], which is directly determined as 5%. Based on cumulative distribution function, the minimum p_{min}^c and the maximum p_{max}^c color deviation in red, green, and blue color channels for underwater image is defined as:

$$p_{min}^c = \min \{x | H^c(x) \geq M^* N^* per^c\} \quad (6)$$

$$p_{max}^c = \max \{x | H^c(x) \leq M^* N^* (1 - per^c)\} \quad (7)$$

$$per^c = \alpha \times \frac{\text{Max} \{ \text{Sum}(p_{out}^r(x)), \text{Sum}(p_{out}^g(x)), \text{Sum}(p_{out}^b(x)) \}}{\text{Sum}(p_{out}^c(x))} \quad (8)$$

where H^c is the cumulative histogram corresponding to P_{out}^c in the c channel, and P_{out}^c is the image processed by PICR. per^c is the limited ratio in the c channel and $c \in \{r, g, b\}$. M and N are the row and column of the image, p_{min}^c and p_{max}^c are the minimum and maximum intensity values of the c channel, Sum and Max are function of sum and maximum, respectively. α is a heuristic value and set to 0.002 for each color channel.

1) Global correcting of red, blue, and green channels



FIGURE 4. Color corrected underwater images. From top to bottom: 1. Raw underwater images; 2. Color corrected underwater images by our method.

The color correction method of the output image is applied within a certain range. The proposed method applies limits to the input image instead of limiting the output image. The pixel intensity values of red, green, and blue channels of the input image are limited as

$$p(x)^c = \begin{cases} p_{\min}^c & p(x)^c \leq p_{\min}^c \\ p(x)^c & p_{\min}^c < p(x)^c < p_{\max}^c \\ p_{\max}^c & p(x)^c \geq p_{\max}^c \end{cases} \quad (9)$$

Then, the color correcting process is applied in accordance with formula (10). $p(x)_{CR}^C$ and $p(x)^c$ are the output and input images in the c channel, respectively. p_{\min}^c , p_{\max}^c , o_{\min}^c and o_{\max}^c are the minimum and maximum intensity values of the input and output images in the c channel, respectively.

$$p(x)_{CR}^C = o_{\min}^c + (p(x)^c - p_{\min}^c) \left(\frac{o_{\max}^c - o_{\min}^c}{p_{\max}^c - p_{\min}^c} \right) \quad (10)$$

Figure 4 shows several examples of corrected results, it shows more color details than underwater degraded images. Although we have no ground truth to verify the accuracy and robustness of the color correction method, the color of underwater images corrected by the proposed method looks more genuine and pleasing than before. Despite this step shows excellent performance in reducing underwater color distortion, it cannot solve the problem of low visibility due to the edges and details of the scene are affected by the scattering problem. Therefore, a local equalization of dual-interval histogram based on average of peak and mean values is employed improve image contrast in the section C.

C. LOCAL EQUALIZATION OF HISTOGRAM

In Figure 4, color corrected underwater images with more genuine and pleasing color. However, the color corrected underwater images still with the problem of low visibility. Therefore, the step aims to enhance image contrast due to the edges and details of the scene are affected by the scattering.

1) CALCULATION THE MINIMUM, MAXIMUM, AND AVERAGE THRESHOLD OF HISTOGRAMS OF RED, GREEN, AND BLUE CHANNELS

First, the minimum, maximum, and average value of the histogram for each channel is calculated. The minimum intensity value i_{\min}^c is calculated based on the lowest intensity value of the image histogram, whereas the maximum intensity value i_{\max}^c is calculated based on the highest intensity value of the image histogram. The average threshold i_{ave}^c is selected based on average of peak and mean values.

Azmi *et al.* [30] had used the mean point, median point, and the average point of the mean and median points as the separation point to divide the histogram into two regions. Different from the separation method of [30], we consider that most underwater images are captured with dark areas at the background and bright areas at the foreground. To be precise, the area close to the light source is brighter than the area away from the light source. Therefore, it is necessary for underwater images to be divided into background sub-image and foreground sub-image in our framework. In addition, when the sample size is large and does not include outliers, this mean usually results in better separation performance. However, the peaks give an ideal separation performance for some to be extreme values (high or low). Considering this fact, the proposed method considers that the background and foreground sub-images are separated by an average threshold of peak and mean values for each color channel. The detailed calculation steps are as follows.

Step1: The peak value is calculated by $i_{peak}^c = \text{find}(\mathbf{T}^c == \max(\mathbf{T}^c), 1)$, where \mathbf{T}^c is the number of times each pixel value appears in the image histogram of channel c , the $\max()$ is the function that takes the largest pixel out, and $\text{find}(\mathbf{T}^c == \max(\mathbf{T}^c), 1)$ is the pixel value corresponding to the first peak point to be taken out.

Step2: The mean value is calculated by $i_{mean}^c = \frac{\sum_{i=1}^M \sum_{j=1}^N i^c(i,j)}{M*N}$, M and N are the number of rows and columns of the input

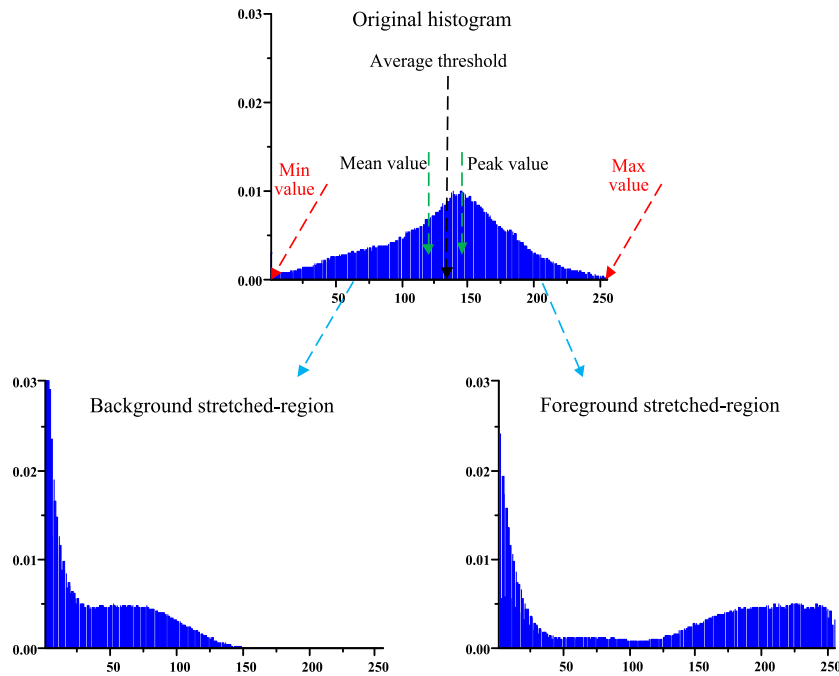


FIGURE 5. Dividing and stretching of the original histogram to produce background-stretched and foreground-stretched regions.

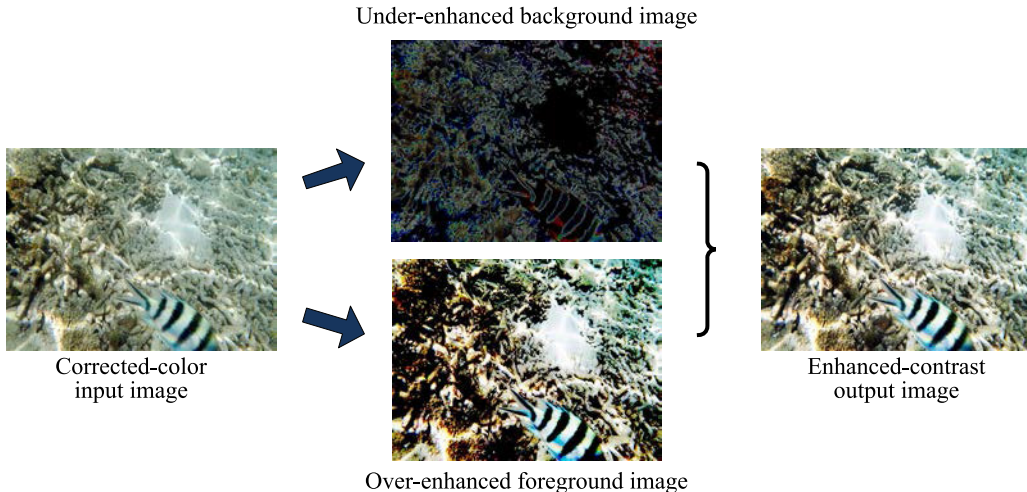


FIGURE 6. Integration process of under-enhanced background image and over-enhanced foreground.

image I , respectively. i_{mean}^c is the mean of the total pixel intensity in the c channel.

Step3: The average threshold is calculated according to the average values of peak and mean, it is expressed as $i_{ave}^c = \frac{(i_{peak}^c + i_{mean}^c)}{2}$.

2) LOCAL ENHANCING OF RED, BLUE, AND GREEN CHANNELS

After the average threshold is determined, the histogram of each color channel (red, green, and blue) is divided into two regions, namely the background and foreground stretched-

regions, as shown in Figure 5. Then, the background region is stretched from the minimum intensity value i_{min}^c to the average threshold i_{ave}^c of the dynamic range, and the foreground region is stretched from the average threshold i_{ave}^c to the maximum intensity value i_{max}^c of the dynamic range.

The background and foreground regions are stretched by Eq. (11) and Eq. (12), respectively.

$$p_B^c = i_{min}^c + (i_{ave}^c - i_{min}^c) \times CDF(i_n^c), \quad i_n^c \in [0, i_{ave}^c] \quad (11)$$

$$p_F^c = (i_{ave}^c + 1) + (i_{max}^c - (i_{ave}^c + 1)) \times CDF(i_n^c), \\ i_n^c \in [i_{ave}^c, 255] \quad (12)$$

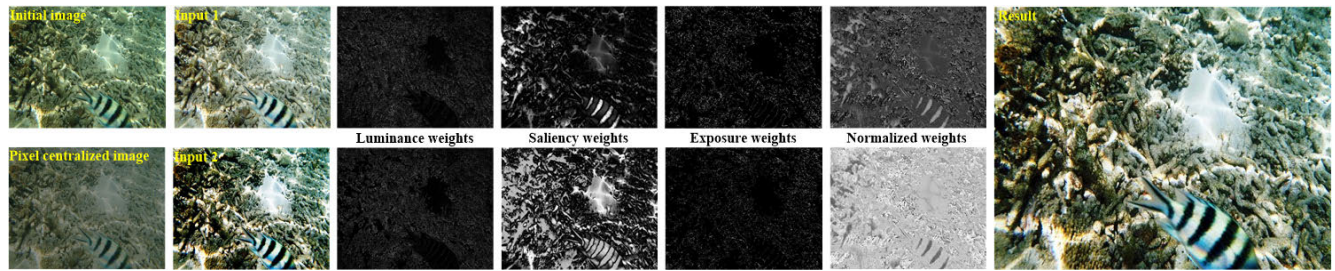


FIGURE 7. Input images from the PICR, contrast weight map, saliency weight map, exposure weight map and normalized weight map or each input images, and our final result.

where p_B^c and p_F^c are pixels intensity values of the background and the foreground stretched-regions in the c channel, respectively. i_n^c and $CDF()$ are pixel values and cumulative distribution function, respectively. Meanwhile, $CDF(i_n^c)$ represents the cumulative frequency of pixel value i_n^c from the current position n to the starting position in the c channel.

For the red, green, and blue color channels, the division at the average point and equalization processing will produce two regions, namely lower-stretched background and upper-stretched foreground regions. All low-stretched background regions are composed to produce an under-enhanced background image. Likewise, all upper-stretched background regions are composed to produce an over-enhanced background image. After that, these images are integrated in the average threshold points. Figure 6 shows the integration process of under-enhanced background image and over-enhanced foreground image to output a contrast-enhanced image.

This step has achieved good results in improving contrast. In general, the local equalization of histogram enhanced underwater images tends to appear too bright for some underwater images with high brightness. Therefore, a gamma correction operation is applied to the contrast-enhanced image. This operation increases the difference between darker/lighter areas at the expense of losing detail in under-exposed/over-exposed areas. To compensate for this loss, we adopted a dual-image multi-scale fusion strategy to fuse the color corrected and contrast enhanced images. Where the color corrected image and the contrast enhanced image are derived from the global equalization operation of histogram and the local equalization operation of histogram with gamma correction, respectively. Details of the fusion will be presented in D.

D. DUAL-IMAGE MULTI-SCALE FUSION

Dual-image multi-scale fusion strategy is inspired by [39]. In work of Ancuti et al. [39], a gamma corrected image and a sharpened image are derived from a white-balanced version of the input, and are fused by a fusion method. However, our method differs from Ancuti et al. [39] in the input image of the fusion method. On the one hand, we use a local equalization of histogram to achieve the detail sharpening and contrast enhancement of the image, while using a gamma correction to correct the over-enhancement problem introduced

by the local equalization of histogram for some underwater images with high brightness. On the other hand, we use the color-corrected image as another input of the fusion method to compensate for the loss introduced by gamma correction, and we use the exposure weight map to replace the saturation weight map in Ancuti et al. [39]. As displayed in Figure 2 and detailed below, the underwater image fusion process consists of three parts: two input images, weight maps definition, and dual-image multi-scale fusion.

1) WEIGHT MAPS

In the fusion process, the use of weight maps makes pixels with high weight values more easily represented in the final result (see Figure 7). Therefore, they are defined based on a large number of local image quality or saliency metrics.

Luminance weight map (W_L) is used to estimate the global contrast by applying a Laplacian filter on each input luminance channel and computing the absolute value of the filtering operation, it is expressed as Eq. (13). However, the weight is not sufficient to enhance the contrast of underwater images. To solve this problem, the proposed method introduces a saliency weight and an exposure weight.

$$W_L^k = |LF^*L^k| \quad (13)$$

where LF and $*$ are the Laplace operator and the convolution operation, respectively. L^k is luminance channel of each input I^k .

Saliency weight map (W_S) aims at highlighting the salient objects and increase the contrast between the highlighted area and shaded area, thereby improving the global contrast of the output image. In the LAB color model, the saliency weight maps of input1 and input2 are obtained by Eq. (14).

$$W_s^k = (L^k - L_m^k)^2 + (a^k - a_m^k)^2 + (b^k - b_m^k)^2 \quad (14)$$

When $k = 1$, L^1 , a^1 , and b^1 are the luminance and color channel values of a and b of the input image I^1 , respectively. L_m^1 , a_m^1 , and b_m^1 correspond to the average of the L^1 , a^1 , and b^1 , respectively. Likewise, the image I^2 can be understood when $k = 2$.

Exposure weight map (W_E) reduces the color cast by processing the saturation gain of the blurred image for the color shift problem of underwater images. In the LAB color model, the exposure weight maps of input1 and input2 are

TABLE 1. Quantitative result of 8 underwater images selected from the DataA. The best result is in bold.

	Red channel [14]			Hybrid-based [17]			UIBLA [18]			GDCP [19]		
	AG	PCQI	UCIQE	AG	PCQI	UCIQE	AG	PCQI	UCIQE	AG	PCQI	UCIQE
Turtle1	5.7025	1.1950	0.5345	6.6687	1.1798	0.3659	7.2294	1.2492	0.3659	5.1053	1.0496	0.3794
Fish1	2.2810	1.0369	0.5356	3.6852	1.1650	0.4258	2.8330	1.1492	0.4258	3.0785	1.1425	0.5764
Fish2	3.9709	1.0184	0.5676	4.0907	0.9474	0.5193	5.3945	0.8560	0.5193	5.8351	0.9680	0.5250
Fish3	3.3864	1.1468	0.5087	5.5308	1.2453	0.3562	3.9831	1.2237	0.3562	3.3282	1.0141	0.3740
Diver1	2.4054	1.0785	0.5547	3.3715	1.0519	0.4230	2.4311	0.9004	0.4230	2.9731	1.0680	0.5924
Diver2	2.5027	1.0743	0.5470	3.6652	1.1292	0.4358	3.4764	1.1546	0.4358	3.9364	1.0931	0.4826
Diver3	3.1289	1.0222	0.5668	4.3913	1.0418	0.4309	3.0939	1.0768	0.4309	5.2446	1.0949	0.6367
Diver4	3.0903	0.9943	0.5843	4.2649	1.0978	0.4136	3.1803	1.0826	0.4136	3.2671	0.9776	0.4534
Average	3.3085	1.0708	0.5499	4.3378	1.1011	0.4213	3.9527	1.0865	0.4213	4.0960	1.0509	0.5024
	Retinex-based [31]			Fusion-based [35]			Two-step [41]			Our method		
	AG	PCQI	UCIQE	AG	PCQI	UCIQE	AG	PCQI	UCIQE	AG	PCQI	UCIQE
Turtle1	7.4178	1.1534	0.3659	5.9823	1.1839	0.5455	7.6837	1.2523	0.4936	7.9224	1.2413	0.5702
Fish1	4.6895	1.1444	0.4258	3.2636	1.1769	0.6198	3.3495	1.1602	0.5226	4.9191	1.2045	0.6639
Fish2	5.6026	1.0633	0.5193	3.7902	0.8715	0.5791	5.6767	1.1575	0.5438	5.3805	1.1170	0.5874
Fish3	5.7045	1.1923	0.3562	4.1440	1.1888	0.5646	4.1497	1.1524	0.4584	6.3707	1.2428	0.6088
Diver1	2.8431	0.9279	0.4230	2.8425	1.0762	0.5836	3.9713	1.0877	0.5475	4.1246	1.1021	0.6181
Diver2	4.1809	1.1031	0.4358	3.3545	1.1618	0.6022	4.5516	1.1859	0.5448	4.7698	1.1959	0.6416
Diver3	4.4018	0.9677	0.4309	3.4277	1.0089	0.5814	5.1666	1.0861	0.5657	5.5701	1.1402	0.6211
Diver4	4.7096	1.0509	0.4136	3.6117	1.0671	0.6055	4.2696	1.0652	0.5473	5.7717	1.1461	0.6458
Average	4.9437	1.0753	0.4213	3.8020	1.0918	0.5852	4.8523	1.1434	0.5279	5.6036	1.1737	0.6196

obtained by Eq. (15).

$$W_E^k = \exp\left(-\frac{(I^k(i,j) - \beta)}{2\sigma^2}\right)^2 \quad (15)$$

where $I^k(i,j)$ is the value of the input image I^k in the pixel location (i,j) , while the mean value β and standard deviation σ are set to 0.5 and 0.25 refer to [60].

Normalized weight map (\bar{W}) yields consistent results. Finally, the normalized weight maps $\bar{W}^k = W^k / \sum_{k=1}^K W^k$, and $W^k = W_L^k + W_s^k + W_E^k$. The normalized weights of corresponding weights are shown in Figure 7.

TABLE 2. Average quantitative result of 63 tested underwater images DataA. The best result is in bold.

Method	AG	PCQI	UCIQE
Red channel [14]	3.3811	1.0327	0.5376
Hybrid-based [17]	5.4876	1.0908	0.4329
UIBLA [18]	4.1098	1.1084	0.4330
GDCP [19]	4.7044	1.0706	0.5317
Retinex-based [31]	5.6068	1.0180	0.4329
Fusion-based [35]	3.9007	1.0418	0.5645
Two-step-based [41]	4.7677	1.0699	0.5245
Our method	7.7157	1.1242	0.6524

2) MULTI-SCALE FUSION

To avoid the undesirable halos in the output image, a dual-image multi-scale fusion method is used to fuse the defined input images with the defined weight maps at every pixel location. The detailed operation is as follows:

Step1: The input image I is decomposed by Laplacian pyramid and defined as $L_l\{I^k(x,y)\}$. The normalized weight map \bar{W}^k is decomposed by Gaussian pyramid and defined as $G_l\{\bar{W}^k(x,y)\}$, and the l represents the l^{th} level.

Step2: The Laplacian pyramid $L_l\{I^k(x,y)\}$ and the Gaussian pyramid $G_l\{\bar{W}^k(x,y)\}$ are fused according to $F_l(x,y) = \sum_{k=1}^N G_l\{\bar{W}^k(x,y)\} L_l\{I^k(x,y)\}$ at every pixel location, where $F_l(x,y)$ represents the Laplacian pyramid of the fusion image.

Step3: Reconstruct the Laplacian pyramid to obtain the final fusion image $F(x,y)$ from the bottom level to the top level. Finally, the enhanced image $F(x,y)$ is obtained by Eq. (16) in the top level.

$$F(x,y) = \sum_{k=1}^K \bar{W}^k(x,y) I^k(x,y) \quad (16)$$

where I^k is the input ($k = 2$ in our work) that is weighted by the normalized weight maps \bar{W}^k .

V. EXPERIMENTAL RESULTS AND ANALYSIS

The performance of the proposed GLHDF method is compared with several state-of-the-art methods namely red channel [14], hybrid-based [17], underwater image restoration based on image blurriness and light absorption (UIBLA) [18], generalization of the dark channel prior for single image restoration (GDCP) [19], Retinex-based [31], fusion-based [35] and two-step-based [41]. The enhancement results of each method are evaluated in terms of qualitative and quantitative. We use the recommended parameter settings to run the source code provided by the authors to produce the best results for an objective evaluation.

In qualitative evaluation, it is mainly evaluated in terms of contrast, visibility, and color. In quantitative evaluation, it is mainly evaluated in terms of average gradient (AG) [34], patch-based contrast quality index (PCQI) [61] and underwater color image quality evaluation (UCIQE) [62]. A high AG value represents the enhanced image with high clarity. A high PCQI value indicates the enhanced image with high

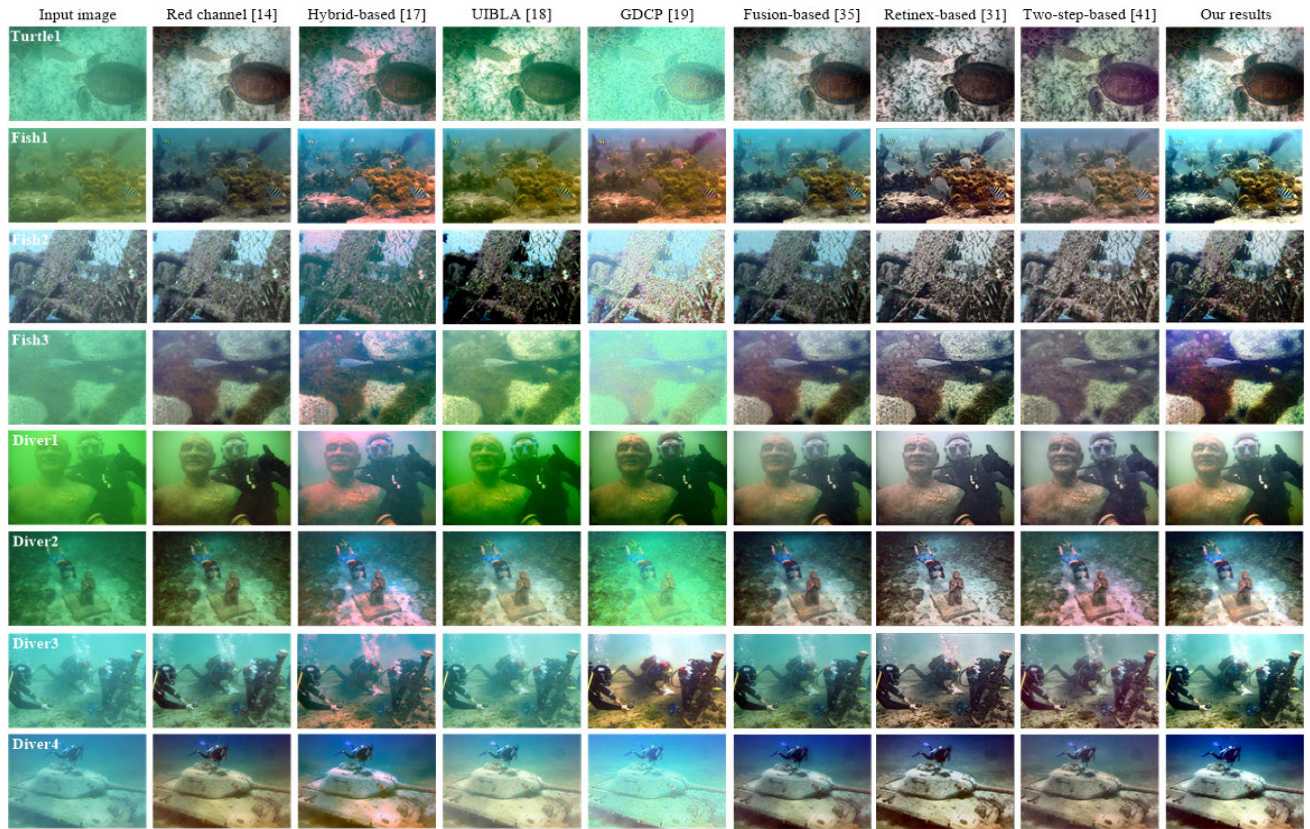


FIGURE 8. Qualitative comparisons on the DataA. Quantitative result of 8 underwater images is provided in Table 1.

TABLE 3. Quantitative result of 8 underwater images selected from the DataB. The best result is in bold.

	Red channel [14]			Hybrid-based [17]			UIBLA [18]			GDCP [19]		
	AG	PCQI	UCIQE	AG	PCQI	UCIQE	AG	PCQI	UCIQE	AG	PCQI	UCIQE
Reef1	11.5726	1.0003	0.5507	16.6950	1.2242	0.4711	14.982	1.2374	0.4711	17.2144	1.0109	0.4834
Reef2	6.9677	0.9854	0.6000	9.0315	1.1408	0.4711	7.1422	1.1508	0.4711	8.9327	1.1182	0.5436
Fish1	3.0396	0.9861	0.5402	4.9411	1.1725	0.4496	3.2559	1.1263	0.4496	4.8350	1.1581	0.5797
Fish2	8.2443	0.9876	0.5774	9.0974	0.9957	0.5403	12.3349	1.0370	0.5403	10.8574	0.9829	0.6313
Fish3	6.7389	1.0289	0.5758	7.0151	0.9708	0.4841	7.8176	1.0812	0.4841	8.6800	1.0292	0.4790
Diver1	5.3633	0.9930	0.5380	8.3962	1.1986	0.4403	6.0443	1.1578	0.4403	7.0631	0.9950	0.4655
Diver2	3.6413	1.0300	0.4921	5.5763	1.1476	0.4404	4.6011	1.1376	0.4404	6.4440	1.1858	0.6100
Diver3	6.2272	0.8969	0.6181	6.5991	0.9132	0.6371	9.4515	1.0518	0.6371	8.8134	0.9139	0.6537
Average	6.4743	0.9885	0.5615	8.4189	1.0954	0.4917	8.2036	1.1224	0.4917	9.1050	1.0492	0.5557
Retinex-based [31]			Fusion-based [35]			Two-step [41]			Our method			
AG	PCQI	UCIQE	AG	PCQI	UCIQE	AG	PCQI	UCIQE	AG	PCQI	UCIQE	
Reef1	15.3595	1.0263	0.4711	12.0525	0.9584	0.57	15.2281	1.2019	0.5044	20.9916	1.2859	0.6323
Reef2	8.6988	1.0233	0.4711	7.0982	0.9616	0.6149	8.0368	1.1059	0.5143	10.9308	1.2082	0.6582
Fish1	5.8881	1.1032	0.4496	3.8455	1.0957	0.5894	3.8996	1.0537	0.4996	5.7472	1.1920	0.6336
Fish2	10.0579	0.9915	0.5403	7.7474	0.9187	0.5595	12.6482	1.1583	0.5537	12.7163	1.1111	0.5994
Fish3	6.9081	0.9829	0.4841	6.8088	1.0466	0.5592	10.7062	1.1968	0.5713	9.2961	1.0884	0.5873
Diver1	8.7328	1.0959	0.4403	6.1229	1.0442	0.5899	7.7243	1.1606	0.5178	10.2842	1.2612	0.6338
Diver2	6.3389	1.1265	0.4404	4.7805	1.1328	0.567	5.2979	1.1809	0.4826	7.2466	1.2078	0.6076
Diver3	7.8382	0.9457	0.6371	5.7021	0.8513	0.6152	9.497	1.0912	0.6394	7.0329	0.8619	0.6353
Average	8.7277	1.0369	0.4917	6.7697	1.0011	0.5831	9.1297	1.1436	0.5353	10.5307	1.1520	0.6234

contrast. A high UCIQE value demonstrates the enhanced image balances chroma, luminance and saturation well.

In this experiment, we evaluate the proposed GLHDF method on real world underwater image datasets DataA, DataB and DataC. Where the DataA including 63 underwater images is collected from the Internet and the DataB containing 893 underwater images is shared by Li *et al.* [57]. In

addition, 8 low-light underwater images selected from the DataB as DataC. These underwater images usually suffer from color cast, lose details and low contrast. Due to the limited space, we only show parts of the experimental results as shown in Figures 8 to 10. Furthermore, Tables 1 to 4 give quantitative results of tested images and all images of DataA and DataB, and Table 5 gives all the evaluation metrics of

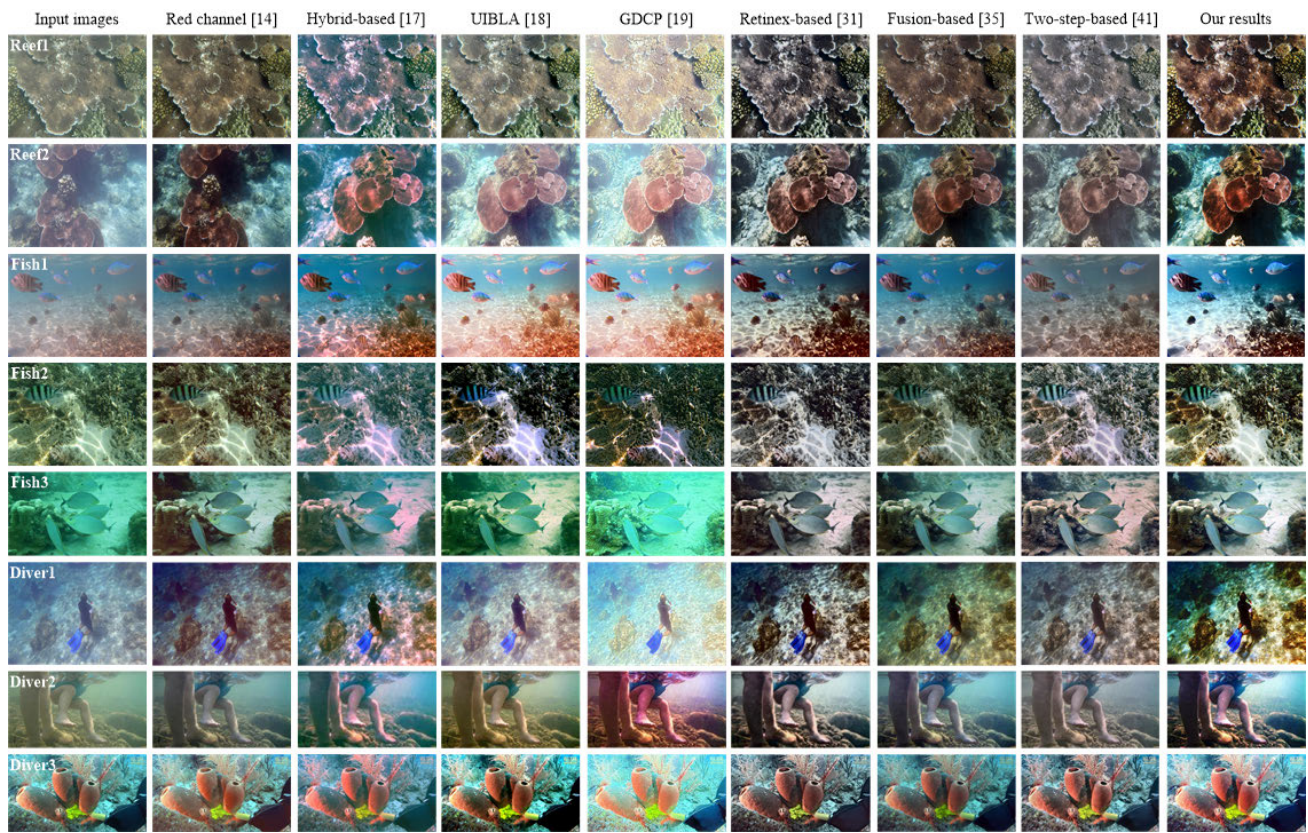


FIGURE 9. Qualitative comparisons on the DataB. Quantitative result of 8 underwater images is provided in Table 3.

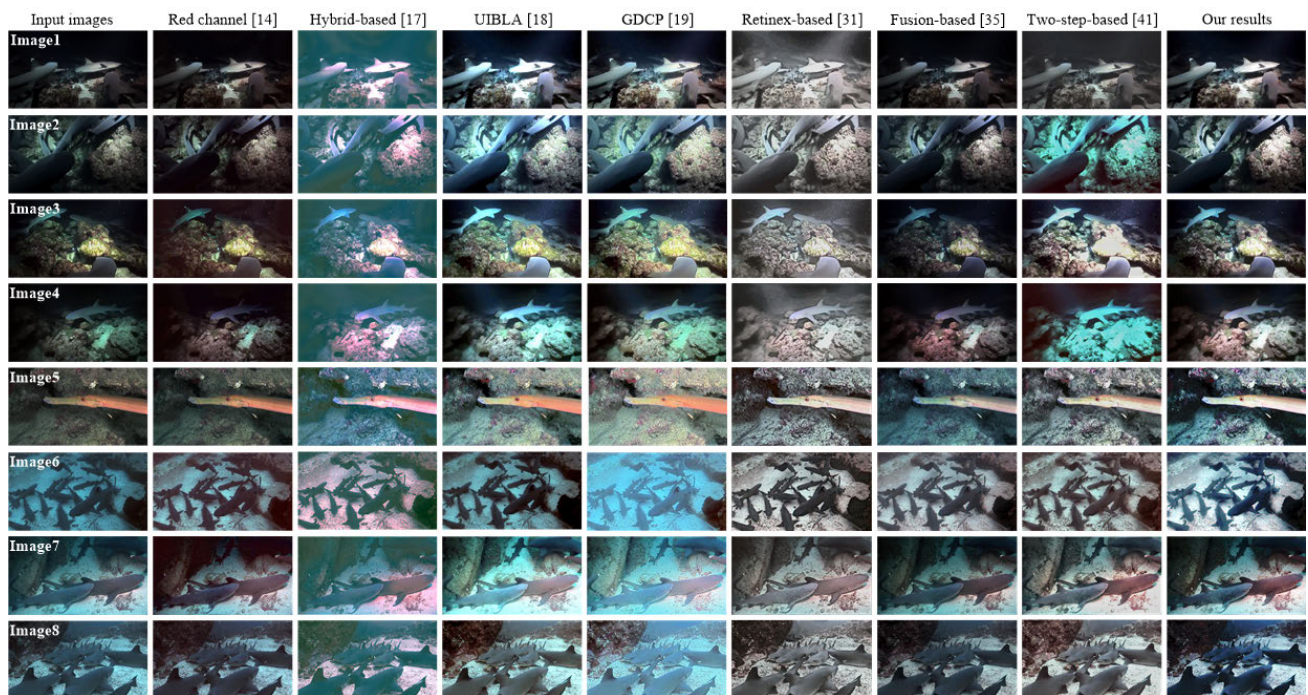


FIGURE 10. Qualitative comparisons on the DataC. Quantitative result of 8 underwater images is provided in Table 5.

DataC. In addition, the proposed GLHDF method is used to enhance the low-light, natural and foggy images captured in the atmospheric environment. Furthermore, the proposed GLHDF method is used to enhance underwater images with a ColorChecker 24 X-Rite Chart captured by different specialized cameras in the same underwater scene.

A. EVALUATION ON DataA

In this part, we evaluate the proposed method on real-world underwater image dataset **DataA**. Due to the limited space, Figure 8 only presents the experimental results of 8 selected images from the DataA.

A first glance at Figure 8 may give the impression that the results of Hybrid-based [17] and Retinex-based [31] might be brighter; however, a careful inspection reveals that the Hybrid-based [17] method causes over-saturation that some results with red tone. Similarly, Retinex-based [31] method leads to a darker appearance. Two-step-based [41] results in a darker appearance that some results with red tone. And the images enhanced by UIBLA [18] and GDCP [19] are not natural and over-enhancement. The methods of Red channel [14] and Fusion-based [35] have little effect. In contrast, the proposed GLHDF method presents promising results on real-world underwater images DataA, without introducing any color casts, artificial, over- and under-enhanced areas.

Observing the failure cases in Figure 8, the Hybrid-based [17] and Two-step-based [41] tend to introduce reddish color in some results. For the failure cases of the Red channel [14], UIBLA [18] and GDCP [19], it aggravates the greenish failure and produces unpleasing results visually. For the failure cases of the Retinex-based [31] and Fusion-based [35], it leads to a darker appearance that some results lost details. In contrast, the proposed GLHDF method removes color casts and improves contrast and brightness of enhanced images, which generates better visibility and pleasant perception.

We first evaluated the AG, PCQI, and UCIQE metrics of 8 selected underwater images from the DataA as shown in Table 1. It can be seen that the GLHDF can obtain the highest or approximately high AG, PCQI and UCIQE values for these 8 underwater images compared with competitive methods. In addition, we also evaluated the average quantitative result of 63 underwater images as shown in Table 2. It can be observed that the GLHDF method obtains higher AG, PCQI and UCIQE values compared with competitive methods. Therefore, the proposed GLHDF method enhanced results with better sharpness, contrast, chroma, luminance and saturation on real-world underwater image from an objective perspective.

B. EVALUATION ON DataB

In this part, we evaluate the proposed method on real-world underwater image dataset **DataB**. Due to the limited space, Figure 9 shows the experimental results of 8 selected images from the **DataB**.

Like the enhanced results of DataA, the results of Hybrid-based [17] and Retinex-based [31] show the bright-coloured impression at first glance; however, Hybrid-based [17] introduces reddish color casts. Similarly, Retinex-based [31] method leads to a darker appearance. The result produced by the UIBLA [18] and GDCP [19] are exacerbate the greenish color and produce visually unpleasing results. The methods of Red channel [14], Fusion-based [35] and Two-step-based [41] have less effect on the inputs than other methods. In contrast, the proposed GLHDF method removes color casts and improves contrast and brightness, which generates better visibility and pleasant perception.

We evaluated the quantitative results of the 8 selected underwater images and all samples of DataB as shown in Table 3 and Table 4, respectively. It can be observed that the proposed GLHDF method obtains higher AG, PCQI and UCIQE values for single underwater image or all tested underwater images compared with competitive methods.

C. EVALUATION ON DataC

To evaluate the performance of the proposed method for low-light underwater images, we conduct experiments on low-light underwater image DataC. Due to the limited space, Figure 10 presents the experimental results of 8 selected images from the DataC.

In Figure 10, the proposed GLHDF method can remove the color shifts and improve the contrast of the low-light underwater images. Moreover, our results are consistent and without flickering artifacts on all selected low-light underwater images. In contrast, the methods of the UIBLA [18], GDCP [19], Fusion-based [35] and Two-step-based [41] produce inconsistent enhancement for all selected low-light underwater images. For instance, for Image2, the methods of the UIBLA [18], GDCP [19], Fusion-based [35] and Two-step-based [41] produce visually unpleasing results and introduce greenish color casts. Hybrid-based [17] and Retinex-based [31] might be brighter; however, the Hybrid-based [17] method introduces red tone. The method of Red channel [14] has little effect on the input images; however, the method lost details. In addition, the proposed can obtain similar or usually higher AG, PCQI and UCIQE values in Table 5. It shows that our approach has a better enhancement capability for low-light underwater images.

TABLE 4. Average quantitative result of 893 tested underwater images DataB. The best result is in bold.

Method	AG	PCQI	UCIQE
Red channel [14]	5.0002	0.9939	0.5760
Hybrid-based [17]	8.4043	1.0374	0.5155
UIBLA [18]	6.2370	1.0740	0.5196
GDCP [19]	7.4631	1.0463	0.5983
Retinex-based [31]	6.8699	0.9699	0.5196
Fusion-based [35]	5.0426	0.9758	0.5804
Two-step-based [41]	7.2953	1.0824	0.5767
Our method	8.5821	1.1092	0.6511

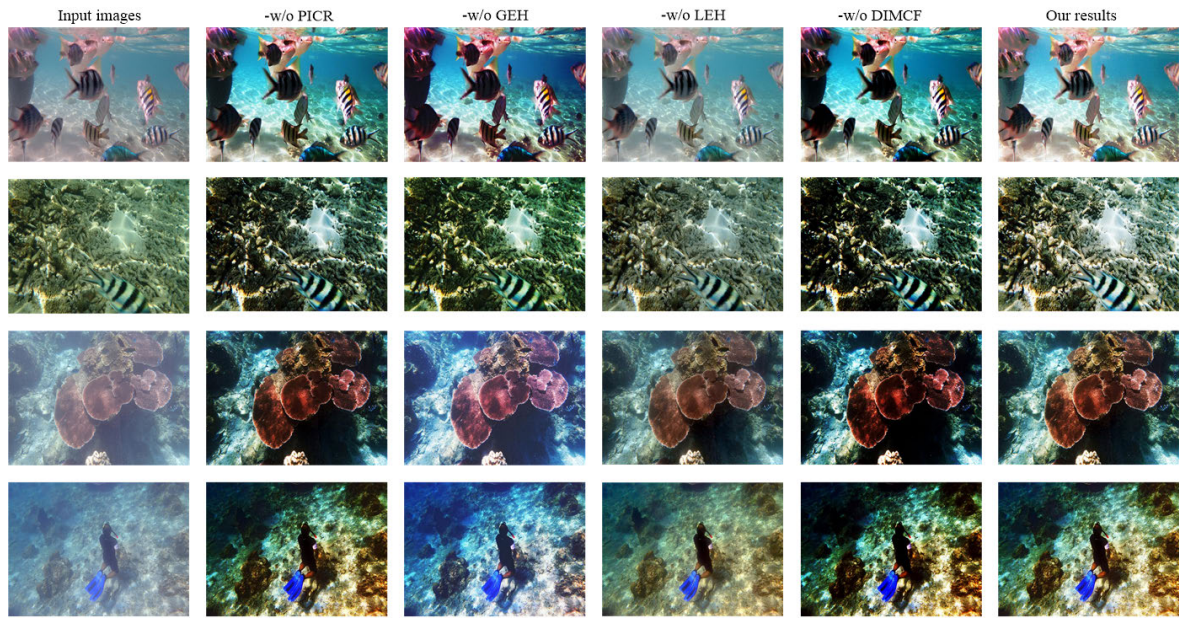


FIGURE 11. Results produced using different components.

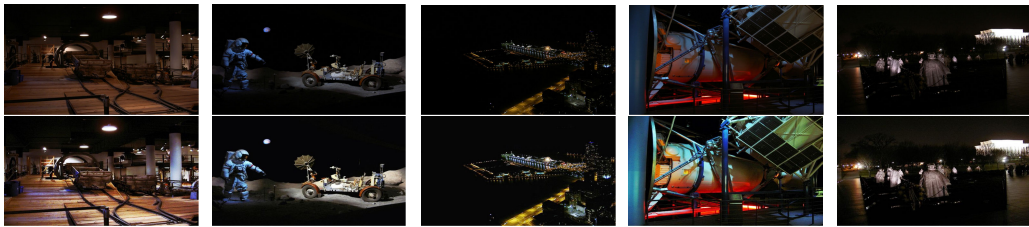


FIGURE 12. Evaluation on low-light images.



FIGURE 13. Evaluation on natural images.



FIGURE 14. Evaluation on foggy images.

D. ABLATION STUDY

To illustrate the effectiveness of each component in the proposed GLHDF method, we conduct an ablation study

including qualitative and quantitative experiments on UIEB. Details as follows: (a) GLHDF without pixel intensity center regionalization (-w/o PICR), (b) GLHDF without global



FIGURE 15. Evaluation on sandy images.

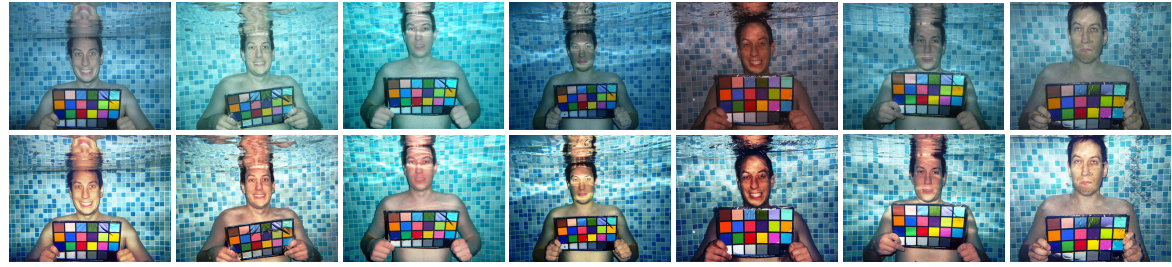


FIGURE 16. The results are obtained via GLHDF (the second row) correspond to underwater images captured by different cameras (the first row). The images are shared by [39]. The cameras used to capture underwater images are Canon D10, FujiFilm Z33, Olympus Tough 6000, Olympus Tough 8000, Pentax W60, Pentax W80, Panasonic TS1, respectively.

TABLE 5. Quantitative result of 8 low-light underwater images. The best result is in bold.

	Red channel [14]			Hybrid-based [17]			UIBLA [18]			GDCP [19]		
	AG	PCQI	UCIQE	AG	PCQI	UCIQE	AG	PCQI	UCIQE	AG	PCQI	UCIQE
Image1	1.0418	0.9973	0.5181	1.4606	0.8113	0.4992	2.0379	1.0141	0.4992	2.1884	1.0311	0.6042
Image2	1.8556	0.9743	0.5228	2.4095	0.8206	0.5349	3.287	0.9833	0.5349	3.7160	1.0133	0.6162
Image3	2.4873	0.9184	0.5729	3.1039	0.8212	0.5863	4.2674	1.0088	0.5863	4.8988	1.0246	0.6360
Image4	1.3091	0.9716	0.5157	1.8634	0.8169	0.5181	2.2031	0.9900	0.5181	2.4403	1.0163	0.5983
Image5	2.2218	0.9865	0.5249	3.6857	0.9843	0.5218	4.0279	1.0368	0.5218	4.6975	0.9636	0.5720
Image6	2.1754	1.0676	0.5721	3.146	1.0086	0.5291	2.1373	1.0840	0.5291	2.3033	0.8545	0.5329
Image7	2.9853	0.9041	0.6076	3.2426	0.8867	0.5580	3.7463	0.9490	0.5580	4.2873	0.9411	0.5464
Image8	4.0856	0.9633	0.5790	4.9310	0.9337	0.5666	5.3609	1.0681	0.5666	5.8125	0.9257	0.5545
Average	2.2702	0.9728	0.5516	2.9803	0.8854	0.5392	3.3834	1.0167	0.5392	3.7930	0.9712	0.5825
Retinex-based [31]			Fusion-based [35]			Two-step [41]			Our method			
AG	PCQI	UCIQE	AG	PCQI	UCIQE	AG	PCQI	UCIQE	AG	PCQI	UCIQE	
Image1	2.1253	0.758	0.4992	1.0552	1.0103	0.5227	1.4113	0.9300	0.4896	1.8336	1.0323	0.5963
Image2	3.2804	0.8829	0.5349	2.2315	1.0313	0.5784	3.2073	0.9741	0.6092	2.8642	1.0404	0.6025
Image3	3.7501	0.8305	0.5863	2.4007	0.9511	0.5534	4.3086	0.9638	0.5905	3.9643	1.0271	0.6150
Image4	2.5009	0.8153	0.5181	1.5282	1.0341	0.5644	2.1351	0.9157	0.6364	3.1846	1.0183	0.6003
Image5	5.1025	1.1033	0.5218	2.9841	1.0434	0.5543	5.7179	1.1636	0.5489	5.2523	1.1298	0.5990
Image6	3.6118	1.0665	0.5291	2.5400	1.0518	0.5479	3.3658	1.1366	0.5540	3.8146	1.0451	0.5927
Image7	3.7217	0.9516	0.5580	2.8923	0.9456	0.5750	4.2478	1.0561	0.5624	3.6898	1.0296	0.6148
Image8	5.0963	0.9705	0.5666	4.2836	0.9642	0.5608	5.3662	1.0459	0.5491	5.8643	1.0561	0.6168
Average	3.6486	0.9223	0.5392	2.4894	1.0039	0.5571	3.7200	1.0232	0.5675	3.8084	1.0473	0.6046

equalization of histogram (-w/o GEH), (c) GLHDF without local equalization of histogram, and (d) GLHDF without dual-image multi-scale fusion. Due to the limited space, Figure 12 only shows part of the UIEB experimental results. The average values in terms of AG, PCQI, and UCIQE are given in Table 6.

From Figure 11, the following observations can be found: 1) Contrast can be enhanced in the test images by the ours-w/o PICR, but the details have not been effectively enhanced. 2) Ours-w/o GEH can enhance contrast, but cannot effectively remove color cast. 3) Ours-w/o LEH can effectively remove color cast, however the contrast is not enhanced well. 3) Our-w/o DIMCF can enhance contrast well, but image details are not obtained. The images produced by the proposed GLHDF

TABLE 6. The corresponding images are presented in Figure 11. The best result is in bold.

Method	AG	PCQI	UCIQE	Averages
-w/o PICR	9.4221	1.0414	0.6477	4.5436
-w/o GEH	9.1004	1.1112	0.6127	4.4808
-w/o LEH	6.8135	1.0778	0.5889	3.9160
-w/o DIMCF	10.2018	0.9899	0.6644	4.4411
Ours	10.9664	1.1656	0.6458	4.8595

method with good visibility, natural color, high contrast, and sharpness texture. Quantitative evaluation results are given in Table 4, GLHDF obtains similar or higher values in terms of AG, PCQI and UCIQE metrics. Additionally, GLHDF

obtains higher averages of AG, PCQI and UCIQE values, which presents the effectiveness of each component.

E. EXTENDED APPLICATIONS

GLHDF is designed to enhance the quality of underwater degraded images. However, the GLHDF is still attempted to enhance the degraded images taken in the atmosphere (low-light, natural, foggy, sandy, and etc.), as shown in Figure 12–14. It can be seen that the images enhanced by the proposed GLHDF method with high contrast, natural color, and clear details.

In addition, we further use underwater degraded images captured by different underwater specialized cameras in the same underwater scene to evaluate the performance of GLHDF, as shown in Figure 16. It can clearly see that the enhanced results by GLHDF with a more satisfying appearance from the subjective perspective.

VI. CONCLUSION

In this paper, the proposed GLHDF method is implemented to improve the quality of real-world and low-light underwater images. GLHDF consists of four stages, namely, pixel intensity center regionalization, global equalization of histogram, local equalization of histogram, and multi-scale fusion. As shown in the result, GLHDF enhanced images with good visibility, natural color, high contrast, and sharpness texture. In addition, the proposed method outperforms other state-of-the-art techniques in qualitative and quantitative. Furthermore, GLHDF also can obtain satisfactory results in terms of low-light, natural, foggy, sandy, and underwater images captured by different underwater specialized cameras.

Despite GLHDF obtains good performance, it also has some limitations. The enhanced images cannot achieve the consistency of the background color for underwater images captured by different underwater specialized cameras in the same scene. The selection of the average threshold of the dual-interval histogram may increase the computational complexity of GLHDF. In addition, GLHDF does not study underwater images taken at different levels of turbidity. We intend to solve the above limitations in future work.

REFERENCES

- [1] H. Lu, Y. Li, L. Zhang, and S. Serikawa, “Contrast enhancement for images in turbid water,” *J. Opt. Soc. Amer. A, Opt. Image Sci.*, vol. 32, no. 5, pp. 886–893, 2015.
- [2] Z. Liang, Y. Wang, X. Ding, Z. Mi, and X. Fu, “Single underwater image enhancement by attenuation map guided color correction and detail preserved dehazing,” *Neurocomputing*, Apr. 2020. [Online]. Available: <https://www.sciencedirect.com/science/article/abs/pii/S0925231220304781>
- [3] H. Lu, J. Guna, and Q. Zhou, “Preface: Optical imaging for extreme environment,” *Opt. Laser Technol.*, vol. 110, p. 1, Feb. 2019.
- [4] M. Han, Z. Lyu, T. Qiu, and M. Xu, “A review on intelligence dehazing and color restoration for underwater images,” *IEEE Trans. Syst., Man, Cybern.*, vol. 50, no. 5, pp. 1820–1832, Jan. 2018.
- [5] W. Zhang, L. Dong, X. Pan, P. Zou, L. Qin, and W. Xu, “A survey of restoration and enhancement for underwater images,” *IEEE Access*, vol. 7, pp. 182259–182279, 2019.
- [6] M. Yang, J. Hu, C. Li, G. Rohde, Y. Du, and K. Hu, “An in-depth survey of underwater image enhancement and restoration,” *IEEE Access*, vol. 7, pp. 123638–123657, 2019.
- [7] T. Treibitz and Y. Y. Schechner, “Active polarization descattering,” *IEEE Trans. Pattern Anal. Mach. Intell.*, vol. 31, no. 3, pp. 385–399, Mar. 2009.
- [8] B. Huang, T. Liu, H. Hu, J. Han, and M. Yu, “Underwater image recovery considering polarization effects of objects,” *Opt. Express*, vol. 24, pp. 9826–9838, May 2016.
- [9] K. O. Amer, M. Elbouaz, A. Alfalou, C. Brosseau, and J. Hajjami, “Enhancing underwater optical imaging by using a low-pass polarization filter,” *Opt. Express*, vol. 24, no. 27, pp. 9826–9838, Jan. 2019.
- [10] K. He, J. Sun, and X. Tang, “Single image haze removal using dark channel prior,” *IEEE Trans. Pattern Anal. Mach. Intell.*, vol. 33, no. 12, pp. 2341–2353, Dec. 2011.
- [11] K. He, J. Sun, and X. Tang, “Guided image filtering,” *IEEE Trans. Pattern Anal. Mach. Intell.*, vol. 35, no. 6, pp. 1397–1409, Jun. 2013.
- [12] Q. Wu, J. Zhang, W. Ren, W. Zuo, and X. Cao, “Accurate transmission estimation for removing haze and noise from a single image,” *IEEE Trans. Image Process.*, vol. 29, pp. 2583–2597, 2020.
- [13] J. Y. Chiang and Y.-C. Chen, “Underwater image enhancement by wavelength compensation and dehazing,” *IEEE Trans. Image Process.*, vol. 21, no. 4, pp. 1756–1769, Apr. 2012.
- [14] A. Galdran, D. Pardo, A. Picón, and A. Alvarez-Gila, “Automatic red-channel underwater image restoration,” *J. Vis. Commun. Image Represent.*, vol. 26, pp. 132–145, Jan. 2015.
- [15] P. L. J. Drews, Jr., E. R. Nascimento, S. S. C. Botelho, and M. F. M. Campos, “Underwater depth estimation and image restoration based on single images,” *IEEE Comput. Graph. Appl.*, vol. 36, no. 2, pp. 24–35, Mar. 2016.
- [16] C.-Y. Li, J.-C. Guo, R.-M. Cong, Y.-W. Pang, and B. Wang, “Underwater image enhancement by dehazing with minimum information loss and histogram distribution prior,” *IEEE Trans. Image Process.*, vol. 25, no. 12, pp. 5664–5677, Dec. 2016.
- [17] C. Li, J. Guo, C. Guo, R. Cong, and J. Gong, “A hybrid method for underwater image correction,” *Pattern Recognit. Lett.*, vol. 94, pp. 62–67, Jul. 2017.
- [18] Y.-T. Peng and P. C. Cosman, “Underwater image restoration based on image blurriness and light absorption,” *IEEE Trans. Image Process.*, vol. 26, no. 4, pp. 1579–1594, Apr. 2017.
- [19] Y.-T. Peng, K. Cao, and P. C. Cosman, “Generalization of the dark channel prior for single image restoration,” *IEEE Trans. Image Process.*, vol. 27, no. 6, pp. 2856–2868, Jun. 2018.
- [20] Y. Wang, H. Liu, and L.-P. Chau, “Single underwater image restoration using adaptive attenuation-curve prior,” *IEEE Trans. Circuits Syst. I, Reg. Papers*, vol. 65, no. 3, pp. 992–1002, Mar. 2018.
- [21] M. Yang, A. Sowmya, Z. Wei, and B. Zheng, “Offshore underwater image restoration using reflection-decomposition-based transmission map estimation,” *IEEE J. Ocean. Eng.*, vol. 45, no. 2, pp. 521–533, Apr. 2019.
- [22] D. Berman, D. Levy, S. Avidan, and T. Treibitz, “Underwater single image color restoration using haze-lines and a new quantitative dataset,” *IEEE Trans. Pattern Anal. Mach. Intell.*, early access, Mar. 2, 2020, doi: [10.1109/TPAMI.2020.2977624](https://doi.org/10.1109/TPAMI.2020.2977624).
- [23] Y. Zhou, Q. Wu, K. Yan, L. Feng, and W. Xiang, “Underwater image restoration using color-line model,” *IEEE Trans. Circuits Syst. Video Technol.*, vol. 29, no. 3, pp. 907–911, Mar. 2019.
- [24] D. Akkaynak and T. Treibitz, “Sea-thru: A method for removing water from underwater images,” in *Proc. IEEE Conf. Comput. Vis. Pattern Recognit. (CVPR)*, Jun. 2019, pp. 1682–1691.
- [25] K. Iqbal, M. Odetayo, A. James, R. A. Salam, and A. Z. H. Talib, “Enhancing the low quality images using unsupervised colour correction method,” in *Proc. IEEE Int. Conf. Syst., Man Cybern.*, Oct. 2010, pp. 1703–1709.
- [26] A. S. Abdul Ghani and N. A. Mat Isa, “Underwater image quality enhancement through integrated color model with Rayleigh distribution,” *Appl. Soft Comput.*, vol. 27, pp. 219–230, Feb. 2015.
- [27] A. S. A. Ghani and N. A. M. Isa, “Enhancement of low quality underwater image through integrated global and local contrast correction,” *Appl. Soft Comput.*, vol. 37, pp. 332–344, Dec. 2015.
- [28] A. S. A. Ghani and N. A. M. Isa, “Automatic system for improving underwater image contrast and color through recursive adaptive histogram modification,” *Comput. Electron. Agricult.*, vol. 141, pp. 181–195, Sep. 2017.
- [29] A. S. A. Ghani, “Image contrast enhancement using an integration of recursive-overlapped contrast limited adaptive histogram specification and dual-image wavelet fusion for the high visibility of deep underwater image,” *Ocean Eng.*, vol. 162, pp. 224–238, Aug. 2018.

- [30] K. Z. M. Azmi, A. S. A. Ghani, Z. M. Yusof, and Z. Ibrahim, "Natural-based underwater image color enhancement through fusion of swarm-intelligence algorithm," *Appl. Soft Comput.*, vol. 85, Dec. 2019, Art. no. 105810.
- [31] X. Fu, P. Zhuang, Y. Huang, Y. Liao, X.-P. Zhang, and X. Ding, "A retinex-based enhancing approach for single underwater image," in *Proc. IEEE Int. Conf. Image Process. (ICIP)*, Oct. 2014, pp. 4572–4576.
- [32] S. Zhang, T. Wang, J. Dong, and H. Yu, "Underwater image enhancement via extended multi-scale retinex," *Neurocomputing*, vol. 245, no. 5, pp. 1–9, Jul. 2017.
- [33] C. Tang, U. F. von Lukas, M. Vahl, S. Wang, Y. Wang, and M. Tan, "Efficient underwater image and video enhancement based on retinex," *Signal, Image Video Process.*, vol. 13, no. 5, pp. 1011–1018, Feb. 2019.
- [34] W. Zhang, L. Dong, X. Pan, J. Zhou, L. Qin, and W. Xu, "Single image defogging based on multi-channel convolutional MSRCR," *IEEE Access*, vol. 7, pp. 72492–72504, 2019.
- [35] C. O. Ancuti, C. Ancuti, T. Haber, and P. Bekaert, "Fusion-based restoration of the underwater images," in *Proc. IEEE Int. Conf. Image Process.*, Sep. 2011, pp. 1557–1560.
- [36] T. Treibitz and Y. Y. Schechner, "Turbid scene enhancement using multi-directional illumination fusion," *IEEE Trans. Image Process.*, vol. 21, no. 11, pp. 4662–4667, Nov. 2012.
- [37] C. Ancuti, C. O. Ancuti, T. Haber, and P. Bekaert, "Enhancing underwater images and videos by fusion," in *Proc. IEEE CVPR*, Jun. 2012, pp. 81–88.
- [38] H. Lu, Y. Li, S. Nakashima, H. Kim, and S. Serikawa, "Underwater image super-resolution by descattering and fusion," *IEEE Access*, vol. 5, pp. 670–679, 2017.
- [39] C. O. Ancuti, C. Ancuti, C. De Vleeschouwer, and P. Bekaert, "Color balance and fusion for underwater image enhancement," *IEEE Trans. Image Process.*, vol. 27, no. 1, pp. 379–393, Jan. 2018.
- [40] H. Lu, Y. Li, X. Xu, J. Li, Z. Liu, X. Li, and S. Serikawa, "Underwater image enhancement method using weighted guided trigonometric filtering and artificial light correction," *J. Vis. Commun. Image Represent.*, vol. 38, pp. 504–516, Jul. 2016.
- [41] X. Fu, Z. Fan, and M. Ling, "Two-step approach for single underwater image enhancement," in *Proc. IEEE Int. Symp. Intell. Signal Process. Commun. Syst.*, Nov. 2017, pp. 789–794.
- [42] K. Nomura, D. Sugimura, and T. Hamamoto, "Underwater image color correction using exposure-bracketing imaging," *IEEE Signal Process. Lett.*, vol. 25, no. 6, pp. 893–897, Jun. 2018.
- [43] S.-B. Gao, M. Zhang, Q. Zhao, X.-S. Zhang, and Y.-J. Li, "Underwater image enhancement using adaptive retinal mechanisms," *IEEE Trans. Image Process.*, vol. 28, no. 11, pp. 5580–5595, Nov. 2019.
- [44] C. O. Ancuti, C. Ancuti, C. De Vleeschouwer, and M. Sbert, "Color channel transfer for image dehazing," *IEEE Signal Process. Lett.*, vol. 26, no. 9, pp. 1413–1417, Sep. 2019.
- [45] C. O. Ancuti, C. Ancuti, C. De Vleeschouwer, and M. Sbert, "Color channel compensation (3C): A fundamental pre-processing step for image enhancement," *IEEE Trans. Image Process.*, vol. 29, pp. 2653–2665, 2020.
- [46] X. Pan, L. Li, H. Yang, Z. Liu, J. Yang, L. Zhao, and Y. Fan, "Accurate segmentation of nuclei in pathological images via sparse reconstruction and deep convolutional networks," *Neurocomputing*, vol. 229, pp. 88–99, Mar. 2017.
- [47] W. Ren, J. Zhang, X. Xu, L. Ma, X. Cao, G. Meng, and W. Liu, "Deep video dehazing with semantic segmentation," *IEEE Trans. Image Process.*, vol. 28, no. 4, pp. 1895–1908, Apr. 2019.
- [48] R. Lan, L. Sun, Z. Liu, H. Lu, C. Pang, and X. Luo, "MADNet: A fast and lightweight network for single-image super resolution," *IEEE Trans. Cybern.*, early access, Mar. 4, 2020, doi: 10.1109/TCYB.2020.2970104.
- [49] C. Li, R. Cong, J. Hou, S. Zhang, Y. Qian, and S. Kwong, "Nested network with two-stream pyramid for salient object detection in optical remote sensing images," *IEEE Trans. Geosci. Remote Sens.*, vol. 57, no. 11, pp. 9156–9166, Nov. 2019.
- [50] W. Ren, S. Liu, L. Ma, Q. Xu, X. Xu, X. Cao, J. Du, and M.-H. Yang, "Low-light image enhancement via a deep hybrid network," *IEEE Trans. Image Process.*, vol. 28, no. 9, pp. 4364–4375, Sep. 2019.
- [51] S. Anwar and C. Li, "Diving deeper into underwater image enhancement: A survey," 2019, *arXiv:1907.07863*. [Online]. Available: <http://arxiv.org/abs/1907.07863>
- [52] J. Li, K. A. Skinner, R. M. Eustice, and M. Johnson-Roberson, "WaterGAN: Unsupervised generative network to enable real-time color correction of monocular underwater images," *IEEE Robot. Autom. Lett.*, vol. 3, no. 1, pp. 387–394, Jan. 2018.
- [53] C. Li, J. Guo, and C. Guo, "Emerging from water: Underwater image color correction based on weakly supervised color transfer," *IEEE Signal Process. Lett.*, vol. 25, no. 3, pp. 323–327, Mar. 2018.
- [54] P. Upalvikan, Z. Wu, and Z. Wang, "All-In-One underwater image enhancement using domain-adversarial learning," 2019, *arXiv:1905.13342*. [Online]. Available: <http://arxiv.org/abs/1905.13342>
- [55] X. Chen, J. Yu, S. Kong, Z. Wu, X. Fang, and L. Wen, "Towards real-time advancement of underwater visual quality with GAN," *IEEE Trans. Ind. Electron.*, vol. 66, no. 12, pp. 9350–9359, Dec. 2019.
- [56] Y. Guo, H. Li, and P. Zhuang, "Underwater image enhancement using a multiscale dense generative adversarial network," *IEEE J. Ocean. Eng.*, early access, Jun. 4, 2019, doi: 10.1109/JOE.2019.2911447.
- [57] C. Li, C. Guo, W. Ren, R. Cong, J. Hou, S. Kwong, and D. Tao, "An underwater image enhancement benchmark dataset and beyond," *IEEE Trans. Image Process.*, vol. 29, pp. 4376–4389, 2020.
- [58] C. Li, S. Anwar, and F. Porikli, "Underwater scene prior inspired deep underwater image and video enhancement," *Pattern Recognit.*, vol. 98, Feb. 2020, Art. no. 107038.
- [59] R. Liu, X. Fan, M. Zhu, M. Hou, and Z. Luo, "Real-world underwater enhancement: Challenges, benchmarks, and solutions under natural light," *IEEE Trans. Circuits Syst. Video Technol.*, early access, Jan. 3, 2020, doi: 10.1109/TCSVT.2019.2963772.
- [60] X. Fu, D. Zeng, Y. Huang, Y. Liao, X. Ding, and J. Paisley, "A fusion-based enhancing method for weakly illuminated images," *Signal Process.*, vol. 129, pp. 82–96, Dec. 2016.
- [61] S. Wang, K. Ma, H. Yeganeh, Z. Wang, and W. Lin, "A patch-structure representation method for quality assessment of contrast changed images," *IEEE Signal Process. Lett.*, vol. 22, no. 12, pp. 2387–2390, Dec. 2015.
- [62] M. Yang and A. Sowmya, "An underwater color image quality evaluation metric," *IEEE Trans. Image Process.*, vol. 24, no. 12, pp. 6062–6071, Dec. 2015.



and imaging systems.

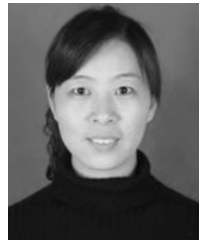
LINFENG BAI received the B.S. degree in control engineering from the Henan University of Science and Technology, Kaifeng, China, in 2010, and the M.S. degree in computer science and technology from the Huazhong University of Science and Technology, Wuhan, China, in 2013. He is currently a Senior Laboratory Teacher with the School of Information Engineering, Henan Institute of Science and Technology. His main research interests include computer vision, image enhancement,



WEIDONG ZHANG (Student Member, IEEE) received the B.S. degree in computer science and technology from the Xinke College, Henan Institute of Science and Technology, Xinxiang, China, in 2015, and the M.S. degree in computer science and technology from the Guilin University of Electronic Technology, Guilin, China, in 2018. He is currently pursuing the Ph.D. degree in information and communication engineering with Dalian Maritime University, Dalian, China. He has authored (coauthored) eight research articles. His main research interests include image enhancement and defogging, and target recognition.



XIPENG PAN received the B.S. degree in automation and the M.S. degree in pattern recognition and intelligent system from the Guilin University of Electronic Technology, Guilin, China, in 2007 and 2013, respectively, and the Ph.D. degree in control science and engineering from the Beijing University of Posts and Telecommunications, China, in 2019. He is currently a Lecturer with the Guilin University of Electronic Technology. His research interests include machine learning, digital image processing, and medical image analysis. He has published more than ten articles.



CHENPING ZHAO received the B.S. and M.S. degrees from the School of Mathematics and Statistics, Henan University, Kaifeng, in 2003 and 2006, respectively, and the Ph.D. degree in applied mathematics from the School of Mathematics and Statistics, Xidian University, Xi'an, in 2018. She is currently a Teacher with the School of Mathematical Science, Henan Institute of Science and Technology. Her research interests include variation method and optimization algorithm for image processing.

• • •